Aqueous KOH Etching of Silicon (110)

Etch Characteristics and Compensation Methods for Convex Corners

Byungwook Kim* and Dong-il Dan Cho

School of Electrical Engineering, College of Engineering, Seoul National University, Seoul 151-742, Korea

ABSTRACT

This paper investigates the anistropic etching characteristics and convex corner undercut mechanism of (110)-oriented silicon in aqueous potassium hydroxide solutions. First, the crystal planes governing the etch front of the undercut are determined, and their etch rates are measured. Then, based on the measured data, several methods for convex corner compensation techniques are examined. Conventionally, <111> direction beams are used to compensate for the undercut on convex corners. This method is found to produce good results for acute convex corners, but results in the emergence of large residue structures with (111) crystal planes on the obtuse convex corners. To alleviate this problem, new corner compensation methods that use triangular and rhombic patterns are developed based on the measured etch front planes. The effectiveness of the proposed corner compensation patterns in reducing the undercut and residues is evaluated in detail. It is found that for obtuse convex corners the rhombic corner compensation provides the best result, and for acute convex corners both the rhombic and <111> beam patterns are effective.

Introduction

Anisotropic etching of single-crystal silicon plays an important role in the fabrication of microstructures. A variety of sharply defined microstructures can be fabricated in single-crystal silicon, owing to the high selectivity between (110) and (111) crystal planes in alkaline etchants. However, this technique cannot be always effective in fabrication of complex 3D structures, because of lateral undercut on convex corners. Although most studies on anisotropic wet etching and convex corner compensation are related to (100)-oriented silicon wafers, deep vertical features cannot be fabricated using (100)-oriented silicon due to the emergence of the slow-etching sidewalls of (111) crystal planes during wet etching.[1-7] On the other hand, deep and sharp vertical furrows, levees, beams, and mesas are easily obtained using (110)-oriented silicon.[6-11] However, there have been comparatively fewer quantitative analyses of the etch characteristics for (110)-oriented silicon necessary for sharply defining the corners of the microstructures. This paper presents a quantitative analysis of silicon (110) etch characteristics and develops suitable compensation methods for sharply defining convex corners.

Establishing the Etch Rates of Silicon (110) in Aqueous KOH

Although there have been many reports concerning the etch rates of (110)-oriented silicon, the data contained in Ref. 6-10 differ quite significantly. Thus, the etch rates of (110) and (111) crystal planes and their ratio must be established before proceeding with experiments.

Potassium hydroxide (KOH) is selected as the etchant because of its high selectivity and relative nontoxicity. Two etch conditions are used in the ensuing experiments: 40% aqueous KOH etching at 70°C, and 50% aqueous KOH etching at 80°C. Note that the KOH flakes used are a mixture of 85% KOH and 15% H_2O by weight. Thus, the true weight percentages of the etchants are 34 and 42.5 wt % for the conditions, respectively. In the rest of the manuscript the weight percentage of 85% KOH flakes (i.e., 40 and 50% aqueous KOH) is noted in the text. In figures and tables both types of expressions of KOH percentage are stated for clarity. The (110)-oriented silicon wafers used in this experiment are double-side-polished n-type 4 in. wafers with $525 \pm 25\ \mu m$ thickness and 10 to 30 Ω cm resistivity.

To achieve a high aspect ratio and to minimize the unwanted lateral etching under an etch mask, accurately aligning the photomask to the (111) crystal plane is very important. For accurate alignment, a fan-shaped alignment target pattern[10,11] that consists of 4 mm long, 20 μm wide beams spanning from -5 to $+5°$ is used. Each beam of this target pattern fans out at an angle of 0.1° to one another. After etching this fan pattern sufficiently, the proper alignment direction within 0.05° accuracy can be determined. This direction is the true <111> crystal direction, and photomasks should be aligned parallel to this crystal direction.

For the KOH etch mask, a 1,500 Å stoichiometric low pressure chemical vapor deposition (LPCVD) nitride film, on top of a 500 Å thermally grown buffer oxide layer, is used. The oxide layer growth was done using wet oxidation at 1,000°C for 37 min with 4,500 standard cubic centimeters per minute (sccm) of O_2, 6,750 sccm of H_2, and 200 sccm of trichloroethane, which was preceded by 3 min of preoxidation at the same condition, except that no H_2 was used in the preoxidation stage. The nitride film was deposited by the decomposition of 100 sccm of NH_3 and 30 sccm of dichlorosilane at 300 mTorr and 785°C for 45 min. Note that these recipes are adapted from the standard CMOS process used at our institute.

Figure 1 shows the schematic setup of the KOH wet etching apparatus used in this paper. The aqueous KOH solution is contained in a Pyrex beaker, which is submerged in a digitally temperature controlled water bath. The beaker capacity is 4 L, and the water bath capacity is 14 L. The temperature of the water bath can be controlled to within ± 0.1°C. An additional mercury thermometer is used to measure the actual temperature of the etchant.

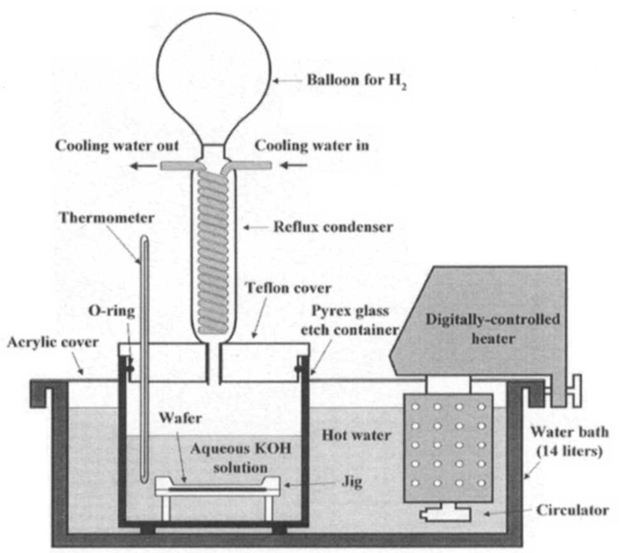

Fig. 1. Experimental setup for the aqueous KOH etching system.

* Electrochemical Society Student Member.

Generally, it takes several hours to stabilize the etchant temperature to a desired one.

To maintain the etchant concentration uniformly throughout the etch process, two approaches are used. First, a large amount of etchant is used. To give the same condition for each experiment, a total weight of 1.5 kg of KOH solution is used in etching a single wafer. By trial and error, involving the measurement of the etch rates of (110) crystal planes at the every hour for 9 h, this amount of the KOH solution is found to be sufficient for maintaining a near constant etchant concentration for a single wafer. Second, a reflux condenser is used to cool down and recollect the outgassing H_2O vapors. At the end of the reflux condenser, a balloon is placed for gathering the H_2 gas.

A series of timed anistropic etching experiments is carried out with a set of test patterns to measure the etch rates of (110) crystal planes and (111) crystal planes for each of the two etch conditions. Table I provides the measured etch rate and selectivity data. Note that these are different than the data in the literature, as the existing data in the literature also differ from one another.[6-10] Also, note that the undercut of the buffer oxide layer under the nitride etch mask is not included in the calculation of the etch rates of (111) crystal planes. Since the etch rate of thermally grown oxide in KOH is not negligible,[6] the true etch rates of (111) crystal planes are lower than those in Table I. Consequently, the true etch rate ratios between the (110) and (111) planes given in Table I are higher. However, since all wafers are prepared with the same etch mask, the data in Table I is used in the rest of this paper.

Convex Corner Undercut Mechanism of Silicon (110)

When micromachining convex corners using (110) silicon in KOH, severe "undercut" takes place. The term undercut indicates the unwanted etching beneath an etch mask, which occurs most severely on the corners of a structure. The dimensions of this corner undercut can be as large as the depth of etch. Thus, in order to fabricate highly defined structures, accurate undercut rates must be known, and suitable corner compensation patterns are necessary.

The convex corner undercut mechanism of (110) silicon is investigated using a parallelogrammic mesa structure bounded by four (111) crystal planes. First, for in situ measurement of the undercut dimensions, graduated test patterns are fabricated. A 500 Å thick buffer oxide is grown on bare (110) wafer, and a 500 Å LPCVD stoichiometric nitride film is deposited. Then, the fan-shaped alignment target is patterned and etched in aqueous KOH to find the true (111) crystal plane. Following this step, grid lines are defined on the nitride film by reactive ion etching (RIE), aligned to the <111> direction. For the grid patterns, 2 μm wide lines parallel to each of the two <111> crystal directions are arranged at every 10 μm. Over the grid lines, a second LPCVD nitride film is deposited at a thickness of 1,500 Å, and the parallelogrammic mesa structures are patterned by RIE aligned to the grid lines. Finally, KOH wet etching at the two conditions is performed. A simplified process flow is depicted in Fig. 2. Note that both nitride layers serve as the etch mask, and the graduated grid lines are used to measure the dimensions of the undercut. With these grid lines, an order of micrometer accuracy can be obtained in the measurements of undercut profiles. This is acceptable because the order of magnitude of the undercut on each convex corner is hundreds of micrometers.

The scanning electron microscope (SEM) photographs of the etched convex corners of the parallelogrammic test structures are shown in Fig. 3. In these SEM pictures, grid-patterned silicon nitride etch masks are partly transparent and bright, and the undercut structures are dark underneath these masks. The major etching front planes that form these undercut angles are observed to be perpendicular to the surface of the wafer. Based on the measurements taken at various etch times, the angles of undercut on each convex corner are calculated as tabulated in Table II. As in this table, all of the etch front planes form an angle of approximately 150.50° with respect to the adjacent (111) crystal planes. As a result, the angles between the normal vectors of (111) planes and the adjacent etch front planes are about 29.50°.

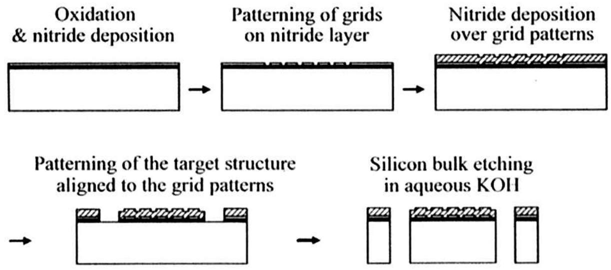

Fig. 2. Simplified process flow for undercut characterization.

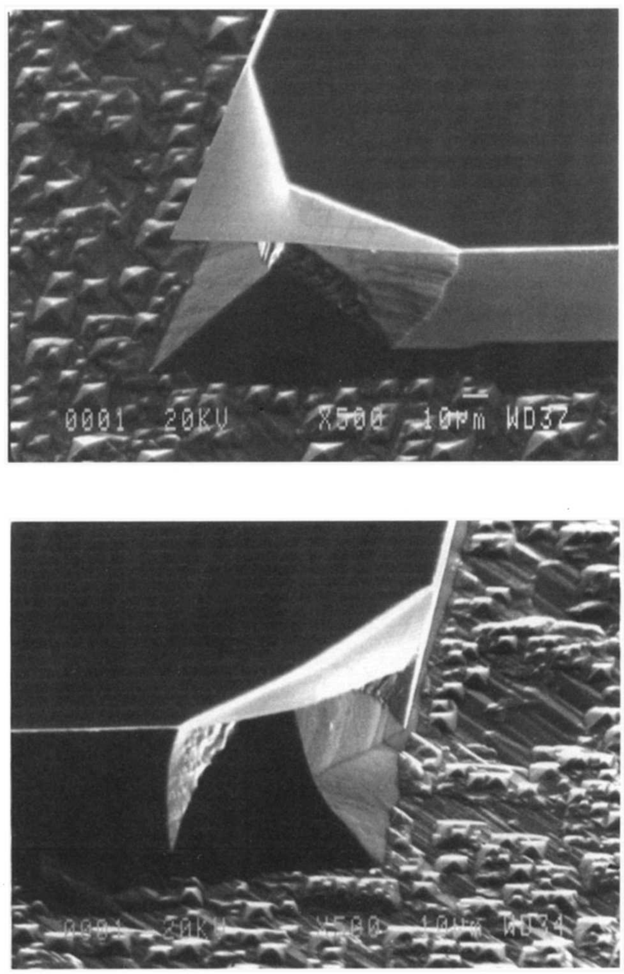

Fig. 3. SEM photographs after 1 h of etching in 40% (34 wt %) 70°C KOH. (a, top) Acute convex corner. (b, bottom) Obtuse convex corner.

Table I. Etch rates and selectives of (110) and (111) crystal planes.

Etch rate / Etch condition	Etch rate of (110) plane, $R_{(110)}$ [μm/h]	Etch rate of (111) plane, $R_{(111)}$ [μm/h]	Selectivity, $R_{(110)}/R_{(111)}$ [μm/h]
40% (34 wt %) 70°C KOH	67.59	1.455	46.45
50% (42.5 wt %) 80°C KOH	93.35	1.174	79.51

Table II. Measured undercut angles of silicon (110).

Etch condition \ Corner	Acute corner parallel to the wafer flat	Acute corner oblique to the wafer flat	Obtuse corner parallel to the wafer flat	Obtuse corner oblique to the wafer flat
40% (34 wt %) 70°C KOH	151.41°	149.98°	150.61°	150.60°
	Mean = 150.69°, [a]std = 1.289°		Mean = 150.61°, std = 1.053°	
50% (42.5 wt %) 80°C KOH	150.37°	150.17°	149.71°	150.84°
	Mean = 150.27°, std = 0.829°		Mean = 150.27°, std = 0.873°	

[a] Std: standard deviation.

From these results, the crystallographic directions of the etch front planes can be calculated. In Fig. 4, the crystallography of (110)-oriented silicon wafer is shown. Figure 4a is the simplified cubic structure of single-crystal silicon, and the diagonal plane indicates a (110) crystal plane. In this diagonal plane, two <111> vectors are indicated. By extending the (110) plane sufficiently, four crystal directions forming about 29.50° with the indicated <111> vectors are found as in Fig. 4b and c. These are <311> and <771> vectors for acute and obtuse convex corners of the parallelogram on a (110) silicon wafer, respectively. This means that the etch front planes are (311) and (771) crystal planes for acute and obtuse corners, respectively. Since these crystallographic directions are identified by the direct in situ measurement using the patterned grid lines, the measured angles can have an error larger than that measured by an exact measurement device using laser reflection. However, we do not have access to such equipment at this time, and we shall refer to these etch front planes as (311) and (771) crystal planes hereinafter. The error associated with this should be minimal. In addition, the most important thing is that the angles between the (111) planes of the convex corners and the planes of the corresponding compensation patterns are 150.50°. In Table III, the etch rates of the (311) and (771) crystal planes are given. These rates are used in developing the new corner compensation methods in this paper.

Conventional Corner Compensation Patterns: <111> Direction Beams

The corner undercut dimensions can be hundreds of micrometers and thus, for sharply defining convex corners, an appropriate corner compensation method is needed. Because the nature of the undercut depends on the crystallography as well as etch conditions, the design of compensation patterns must be specified for each etch condition and the type of wafers (i.e., thickness and orientation) used. Corner compensation methods for (100)-oriented silicon is well known, but so far, the only published method concerning (110)-oriented silicon is that adapted from the method developed for (100)-oriented silicon.[12]

This method uses slender parallelogrammic beam patterns bounded by (111) planes. In this paper, the effectiveness of this method is evaluated first. In order to determine the size of the <111> beam corner compensation patterns, a pre-experiment is performed, in which <111> direction beams with widths of 10 to 200 μm are tested. At every hour of etch, the shortening of the beams is measured for the two etch conditions. The initial lengths of the <111> beams are 3 mm each.

In Fig. 5, a SEM photograph of a 30 μm wide <111> beam etched in 40% KOH at 70°C for 1 h is shown. The undercut occurring at each of the convex corners has shortened the beam by approximately 100 μm. By examining Fig. 5 in detail, the vertical etch mechanism can be inferred as follows: first, the oblique crystal planes are formed at the bottom of the structures, and then the vertical (111) sidewalls appear as the oblique planes are etched away. The oblique planes are (311) planes. The emergence of the oblique (311) planes is also discussed in Krause et al.; these (311) crystal planes are reported to be formed only at KOH concentrations over 30% at 90°C, where $R_{(311)}$ is smaller than $R_{(110)}$.[9] Comparing the etch rates of (311) and (110) planes given in Tables I and III, $R_{(311)}$ is smaller than $R_{(110)}$ for both etch conditions used in this paper, which agrees with the results of Ref. 9. Because of this

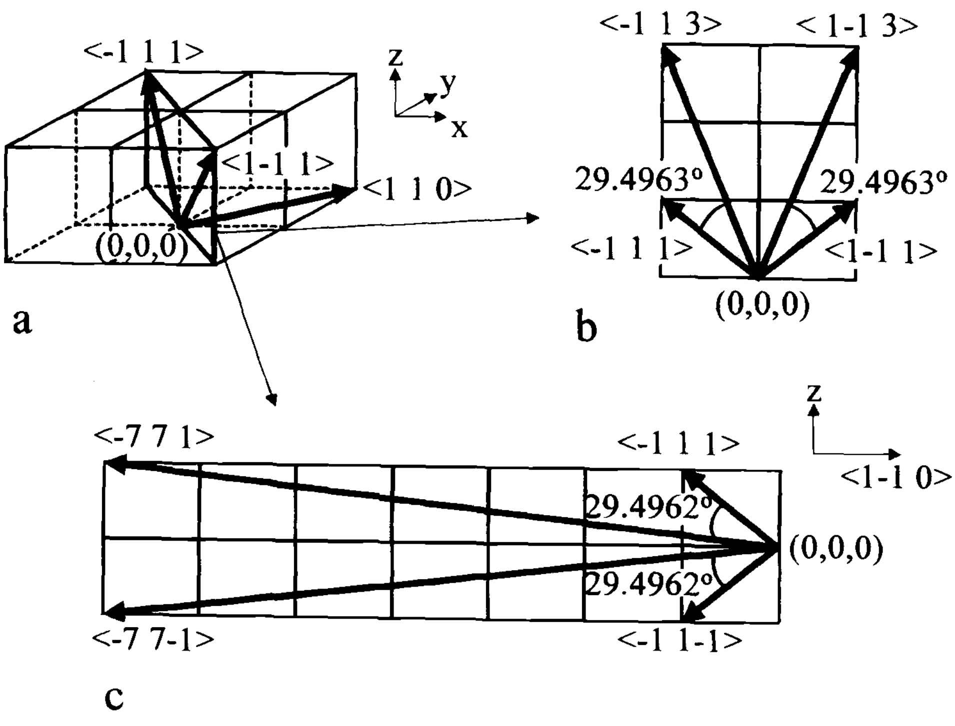

Fig. 4. Crystallography of silicon (110) wafer. (a) Simplified cubic structure of single-crystal silicon. (b) Normal vectors of etch front planes and adjacent (111) planes on acute convex corner. (c) Normal vectors of etch front planes and adjacent (111) planes on obtuse convex corner.

Table III. Etch rates of (311) and (771) crystal planes.

Etch rate / Etch condition	Etch rate of (311) plane, $R_{(311)}$ (measured from acute corner undercut) [μm/h]	Etch rate of (771) plane, $R_{(771)}$ (measured from obtuse corner undercut) [μm/h]
40% (34 wt %) 70°C KOH	53.08	49.32
50% (42.5 wt %) 80°C KOH	63.33	57.19

appearance of the oblique (311) planes, the total etch time required to fabricate a desired depth must be increased.

At this point, it is possible to consider selecting an etch condition, such that the oblique (311) planes do not emerge. However, at such an etch condition, the etch rates of both (110) and (111) planes become very high, and consequently the etch selectivity between (110) and (111) planes becomes very poor, which in turn results in greater undercut and rough surface textures.

Figure 6 illustrates the shortening of the <111> beams as functions of etch time. In each figure, there are 20 graphs. The top of each graph represents the 10 μm wide beam, and the bottom of each graph represents the 200 μm wide beam. As the etch time increases, the lengths of the beams decrease at a constant rate, and this rate does not depend on the width of the beam. As the width gets wider, the graph is simply shifted downward. From the results of this beam etch characterization, the dimensions of the <111> beam corner compensation patterns can be determined.

For the case of 50% 80°C KOH, suppose that an etching time of 8 h is selected. This includes the time to etch away the oblique (311) planes at the bottom. Then using the graph in Fig. 6b, the <111> corner compensation beam length of approximately 900 μm is obtained for the beam width of 100 μm. In etching the compensation test patterns, no significant influence of the beam width to the size and shape of the residue planes on convex corners is observed. This means that any reasonable width over 30 μm is a suitable choice.

Next, the effectiveness of the <111> corner compensation beams in fabricating the convex corners of a mesa structure is evaluated. For this experiment, the width of the compensation beams is fixed at 150 μm. The beam lengths are varied from 700 to 1,500 μm at intervals of 50 μm. In addition, two types of compensation mask are used: one with <111> beams on each of the convex corners parallel to the wafer flat, and the other with <111> beams oblique to the wafer flat at an angle of 70.52°, which is the angle between the two adjacent (111) crystal planes on a (110) silicon wafer. These mask patterns are depicted in Fig. 7.

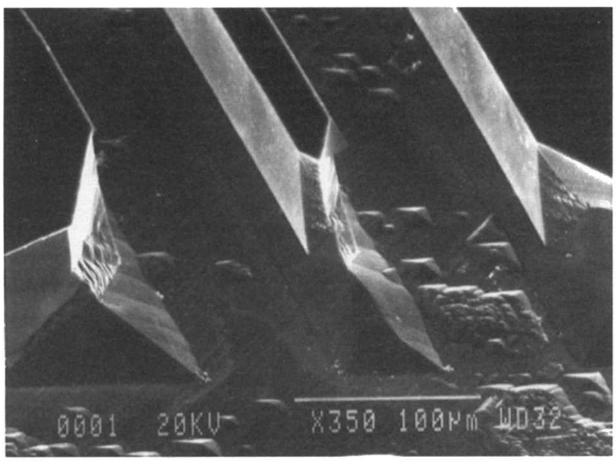

Fig. 5. A SEM photograph of a 30 μm wide <111> direction beam after 1 h of etching in 40% (34 wt %) 70°C KOH.

Figures 8 and 9 are the SEM photographs of the convex corners fabricated using these corner compensation beams. The etch condition is 50% aqueous KOH at 80°C, and the etch time is 8 h. The compensation beam widths are 150 μm for both corners, and the beam lengths are 850 and 900 μm for acute and obtuse corners, respectively. Although the two patterns result in different profiles because of the compensation beam direction, both types are effective for the acute corner in minimizing both the undercut and the residue structure. However, on the obtuse corner, a large residue structure emerges with both types, even though the etch time is sufficiently long. One of the major crystal planes forming these residue structures is a slow etching (111) plane. Thus, the residue structures will not be etched away easily. A conclusion that can be drawn here is that to mini-

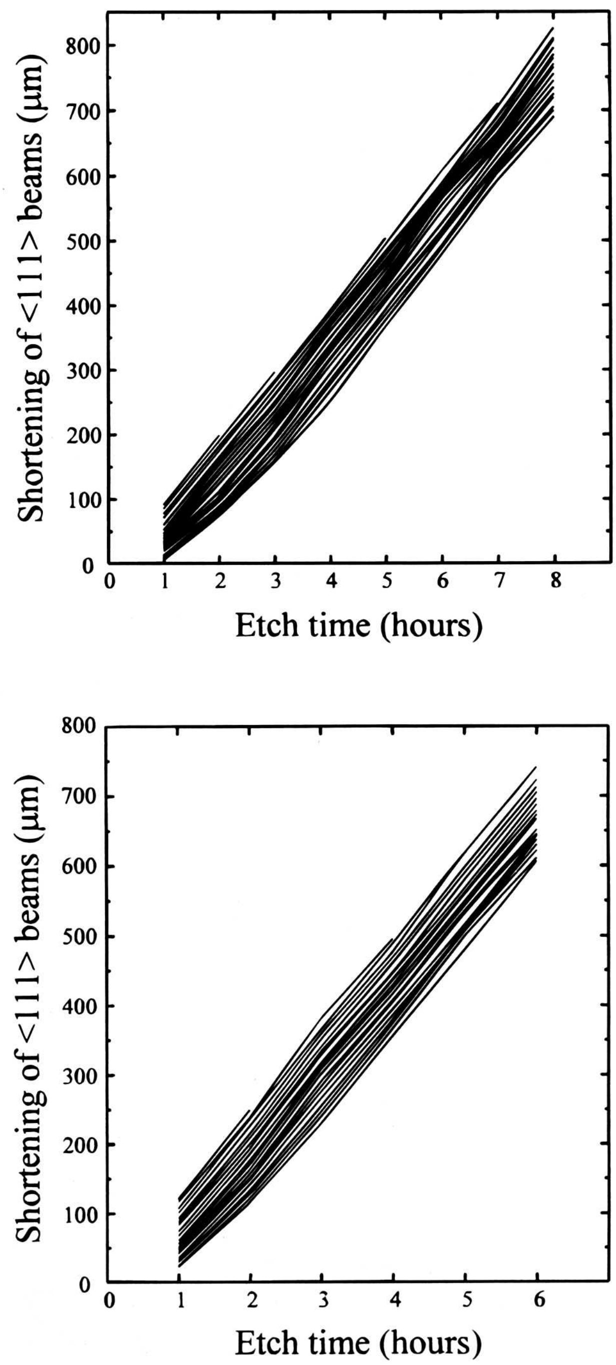

Fig. 6. Shortening of <111> direction beams by undercutting on convex corners. The top of each graph is for 10 μm wide beam down to 200 μm wide beam at the bottom spaced at 10 μm interval. (a, top) 40% (34 wt %) 70°C KOH. (b, bottom) 50% (42.5 wt %) 80°C KOH.

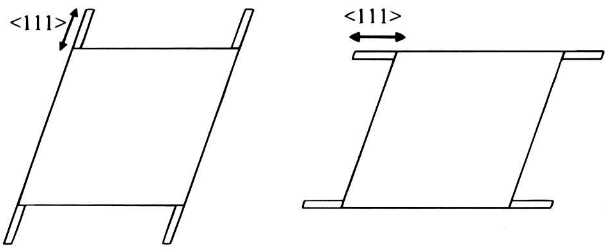

a b

Fig. 7. Conventional compensation patterns: <111> direction slender beams. <111> direction compensation beams: (a) oblique to the wafer flat (b) parallel to the wafer flat.

mize the residue structure on obtuse convex corner, a different compensation method is necessary.

Triangular Compensation Patterns Bounded by (311) and (771) Crystal Planes

The crystal planes governing the convex corner undercut in (110) silicon are found to be (311) and (771) planes for acute and obtuse convex corners, respectively. Based on this, a new triangular compensation method is investigated. The triangular compensation approach is originally proposed by Puers et al. for silicon (100).[1] In this case, the etch front planes governing the undercut on convex corners are (120) or (130) planes depending on the addition of isopropyl alcohol (IPA) to the KOH solution. Using this, triangular compensation patterns bounded by (120) or (130) planes can be devised in order to make square patterns.

However, since the lateral undercut crystallography for silicon (100) is quite different than that for (110)-oriented silicon, new triangular shapes are contrived and tested to compensate for the corner undercut in silicon (110). These corner compensation triangles are bounded by (311) and (771) planes, since these are the etch front planes during the undercut.

In Fig. 10, the schematic of this compensation method is given. On the acute corner, the triangular compensation patterns are bounded by (771) planes, and on the obtuse corner, the triangular patterns are bounded by (311) planes. This is because the obtuse corner undercut angles are used for developing the acute corner compensation triangles and vice versa. As etching is underway, it is expected that those triangular patterns will be etched laterally under the etch mask, and this lateral etching will continue until (111) planes are reached. Consequently, the triangular patterns should be etched away, leaving sharp convex corners formed by the two adjacent (111) planes.

To determine the dimensions of the compensation triangles, the etch rates in Table III are used. Let l_{0a} and l_{0o} be the <771> and <311> direction lateral etch depths, respectively. Then l_{0a} and l_{0o} can be expressed as

$$l_{0a} = R_{(771)} \times \text{etch time}, \quad l_{0o} = R_{(311)} \times \text{etch time} \qquad [1]$$

With these values, the triangle dimensions l_{1a} and l_{1o} in Fig. 10 can be calculated as

$$l_{1a} = \frac{l_{0a}}{\sin 29.50°} \quad l_{1o} = \frac{l_{0o}}{\sin 29.50°} \qquad [2]$$

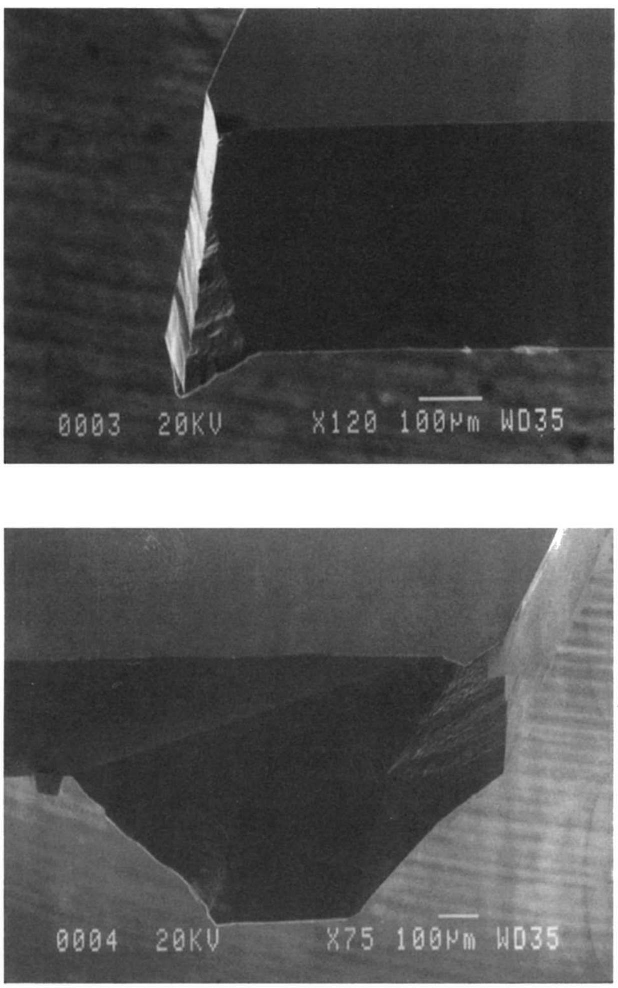

Fig. 8. SEM photographs of the parallelogrammic structures compensated with <111> direction beams oblique to the wafer flat after 8 h of etching in 50% (42.5 wt %) 80°C KOH. (a, top) Acute convex corner. (b, bottom) Obtuse convex corner.

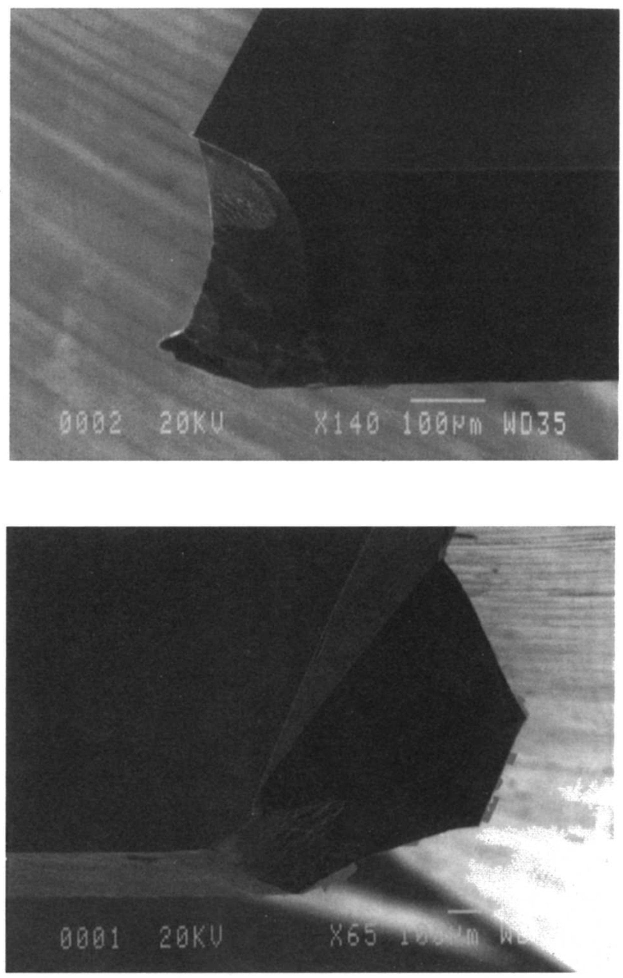

Fig. 9. SEM photographs of the parallelogrammic structures compensated with <111> direction beams parallel to the wafer flat after 8 h of etching in 50% (42.5 wt %) 80°C KOH. (a, top) Acute convex corner. (b, bottom) Obtuse convex corner.

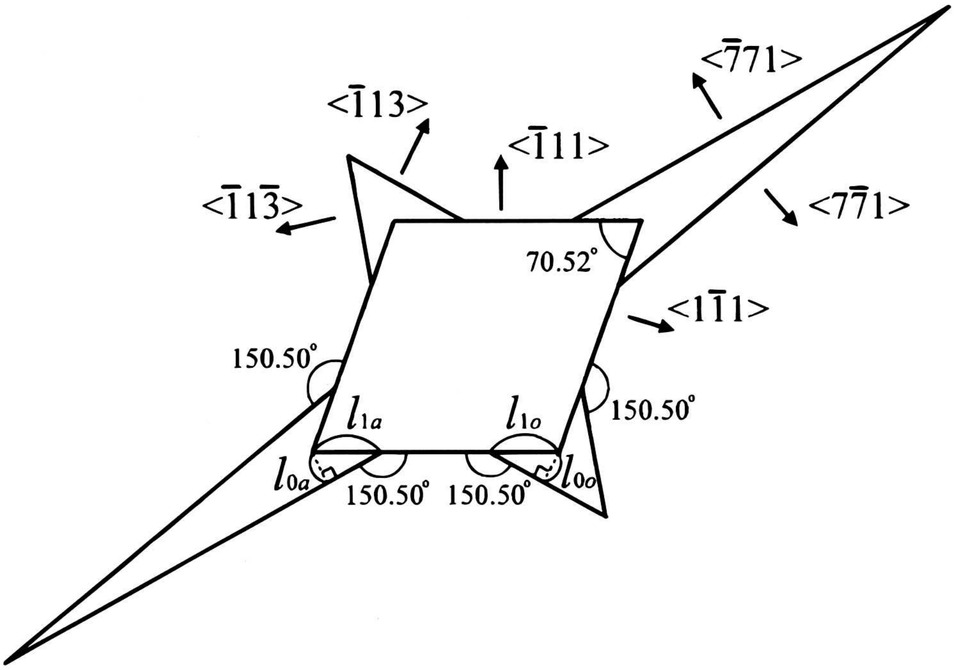

Fig. 10. Triangular compensation patterns bounded by (771) and (311) crystal planes.

Figure 11 shows the results after 8 h of 50% 80°C KOH etch with l_{0a} = 425 μm and l_{0o} = 450 μm. As expected, the top of the structures have very sharp corners with almost no undercut. This shows that the calculation method for the compensation pattern dimensions is correct. However, unacceptably large residue structures remain at the bottom of both acute and obtuse corners, even though the total etch time is sufficiently long. These are, in fact, much bigger than the residues remaining with the <111> beam corner compensation method. In addition, the wafer areas taken up by these triangular corner compensation patterns are too large to be considered practical. Based on the results so far, a new rhombic corner compensation method that compromises between the sharpness at the top and the residue reduction at the bottom, is proposed. The new rhombic compensation patterns also reduce the area requirement substantially.

Rhombic Compensation Patterns Bounded by (111) Crystal Planes

Shortened versions of the triangular compensation method for silicon (100) are reported by Puers et al.[1] In one of these methods, the triangular compensation pattern composed of the (120) or (130) planes is abridged as a rectangular pattern inscribed in the triangular pattern. By creating new 90° convex corners, this rectangle is etched away at the same time as the triangle is consumed. Consequently, the smaller rectangular compensation pattern allows the same compensation effect to be achieved as the larger triangular pattern, while extensive space is saved.

This kind of abridgement can be applied to (110) silicon. However, owing to the quite different crystallography between silicon (100) and (110), the rectangular pattern is substituted by a rhombic pattern. Figure 12 illustrates the rhombic corner compensation patterns for (110) silicon bounded by four (111) crystal planes, developed in this paper. The rhombuses are centered at the vertices of the parallelogram and come into contact with the (311) and (771) triangular corner compensation patterns. Note that the areas occupied by the rhombic structures are much smaller than those of the triangular structures. On each corner of the rhombic compensation structures, <311> and <771> direction undercut will take place, and the rhombuses will be entirely consumed until the etch front

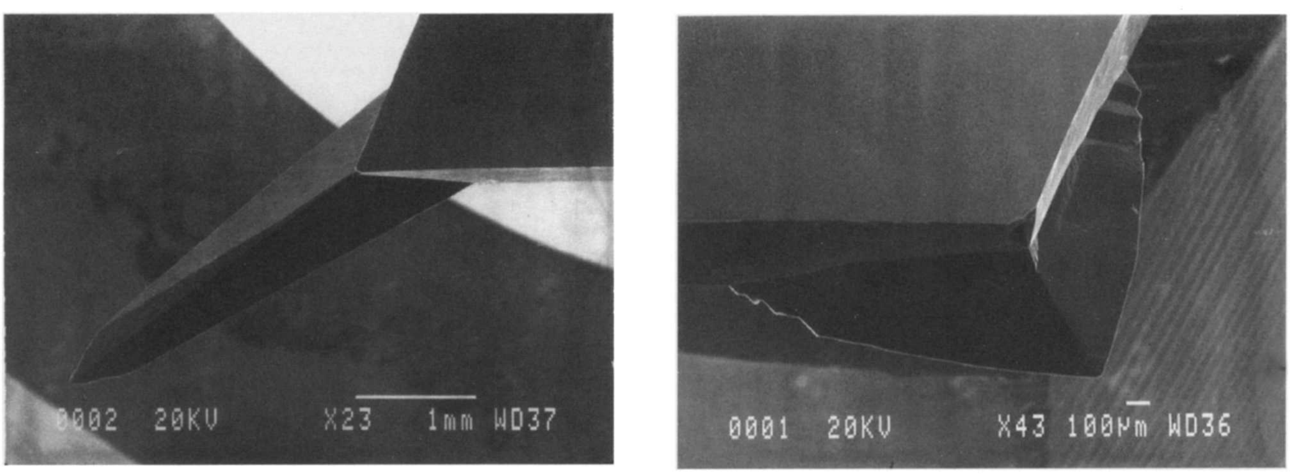

Fig. 11. SEM photographs for triangular compensation patterns bounded by (771) and (311) crystal planes after 8 h of etching in 50% (42.5 wt %) 80°C KOH. (a, left) Acute convex corner. (b, right) Obtuse convex corner.

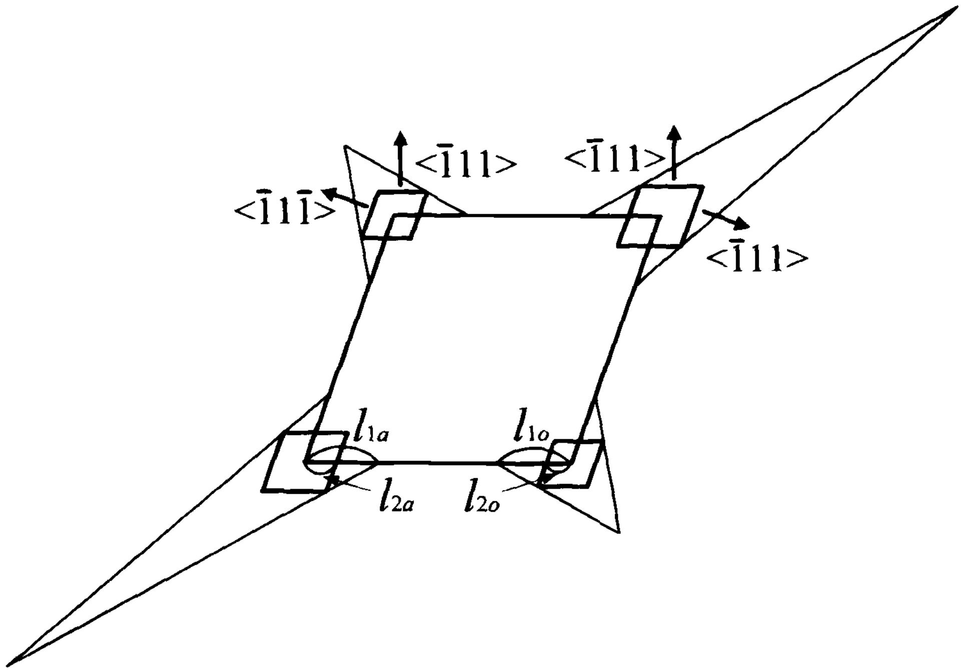

Fig. 12. Rhombic compensation patterns bounded by four (111) crystal planes.

encounters the slow-etching vertical (111) planes. The dimensions of the rhombic patterns are

$$l_{2a} = \frac{\tan 29.50° \times l_{1a}}{\tan 29.50°(1 - \cos 70.52°) + \sin 70.52°}$$

$$l_{2o} = \frac{\tan 29.50° \times l_{1o}}{\tan 29.50°(1 + \cos 70.52°) + \sin 70.52°} \quad [3]$$

where l_{2a} and l_{2o} are one-half of the length of one side of the rhombus on each corner, as indicated in Fig. 12.

The SEM photographs in Fig. 13 and 14 show the progression of etching with the rhombic corner compensation patterns for acute and obtuse corners, respectively. The dimensions of the rhombic patterns are l_{2a} = 300 μm and l_{2o} = 260 μm, which correspond to l_{0a} = 344.63 μm and l_{0o} = 384.06 μm. The etch condition for Fig. 13 and 14 is 40% KOH at 70°C. The final results (Fig. 13e and 14e) show that the residue structures at the bottom are greatly reduced compared to the triangular pattern results, while maintaining relatively sharp features at the top.

To further reduce the residue (111) planes at the bottom, whose etch rate is slower than that of (110) planes, three options are considered. First, since the undercut and the width of the residue structures are dependent on the lengths of the rhombic patterns, moving the rhombuses on the diagonal lines of the parallelogram is experimentally evaluated. However, the results are not good, and for brevity, not included.

The second option is extending the total time to etch away the residues by brute force. However, this is not a good approach, since the lateral undercut in <111> direction will continue in unwanted regions during the extended etch time.

As the third option, reducing the size of the rhombic patterns are considered. In this method a trade-off must be made between the erosion of the upper part by the undercut and the reduction of the residue on the lower part. For example, Fig. 15 shows the results with reduced-size rhombic patterns, optimized for minimizing the residue structures at the bottom. The figure shows that the profiles of the bottom side is very close to the desired shape with no residue structure. However, the erosion by the increased undercut at the top is evident as a trade-off. The etch condition is 50% 80°C KOH, and the etch time is 8 h. For the dimensions of the compensation patterns, l_{2a} is 340 μm and l_{2o} is 300 μm, that correspond to 390.58 μm for l_{0a} and 443.14 μm for l_{0o}. These are about 15% less than the values calculated using Eq. 3.

Discussion

Among the three corner compensation patterns for silicon (110) tested, the newly developed rhombic patterns provide the best results for obtuse convex corners. The results obtained with rhombic patterns (Fig. 14e and 15b) have much sharper profiles with little or no residue structure, compared to the results with the beam pattern (Fig. 8b and 9b) or the triangular pattern (Fig. 11b). Based on these results, it can be concluded that the rhombic corner compensation pattern is the only viable choice for the obtuse corners, among the three compensation patterns considered in this paper.

On acute convex corners, both the beam pattern (Fig. 8a and 9a) and the rhombic pattern (Fig. 13e and 15a) produce good results. The four figures referenced here (Fig. 8a, 9a, 13e, and 15a) have different shapes, and thus, which compensation pattern to choose should be determined depending on the specific needs of applications.

The trade-off between the undercut compensation on the top side and the reduction of the residue structures at the bottom side still remains as a problem. The situation can be alleviated by etching the wafer from both sides, assuming that the photomask can be accurately aligned on both sides of the wafer. As an additional benefit, smaller compensation patterns can be used with the double-side etch technique.

As a final remark, the triangular corner compensation patterns produce the sharpest features at the top side, by not allowing any undercut erosion to take place. Unfortunately, using the double-side etch technique is not effective in eliminating the residue structures in this case, because the residue structural height is too large. It is possible to reduce the size of the triangular patterns, but based on our calculations, the area requirement of the triangular pattern is still larger than that of the rhombic pattern.

Conclusions

This paper presented the etch characteristics of (110)-oriented silicon in aqueous KOH. Etching of parallelogrammic mesa structures defined by (111) planes on the four sides and (110) planes at the top and the bottom was considered. To prevent the undercut on the convex corners, several methods of compensation were investigated. Conventional compensation method with <111> beams was considered first, but the results showed large residue structures on the obtuse corners. Thus, a new triangular corner compensation method, based on the measured etch front planes governing the undercut, was proposed and examined. The triangular patterns bounded by (311) and (771) planes resulted in extremely sharp structures on the top side, almost perfectly compensating for the undercut. However, the undercut prevention resulted in large unwanted residue structures at the bottom side. As a trade-off between the undercut and the residue structures, rhombic corner compensation patterns were proposed and evaluated. In this method, rhombuses are centered at the vertices of the parallelogrammic convex structure and contained within the triangles determined by

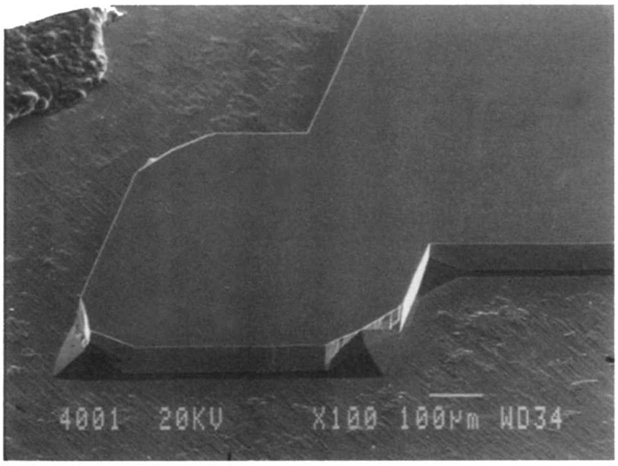

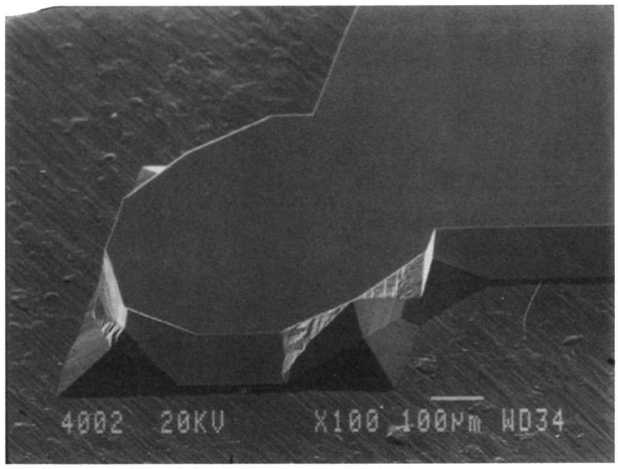

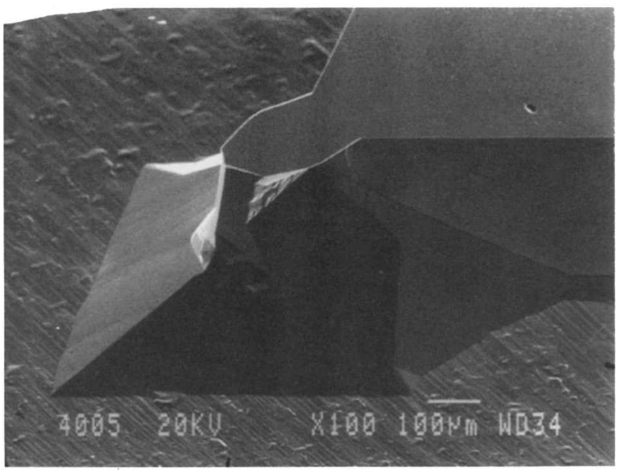

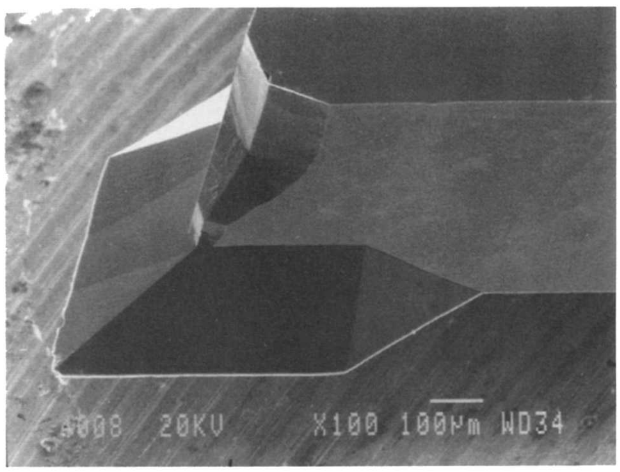

Fig. 13. SEM photographs of acute convex corners of parallelogrammic structures compensated with rhombic patterns bounded by four (111) crystal planes in 40% (34 wt %) 70°C KOH after etching for: (a, top left) 1 h, (b, top right) 2 h, (c, above) 5 h, (d, middle right) 8 h, and (e, bottom) 9 h.

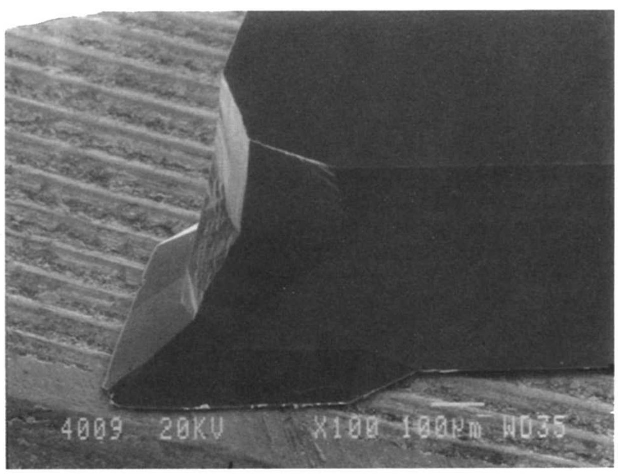

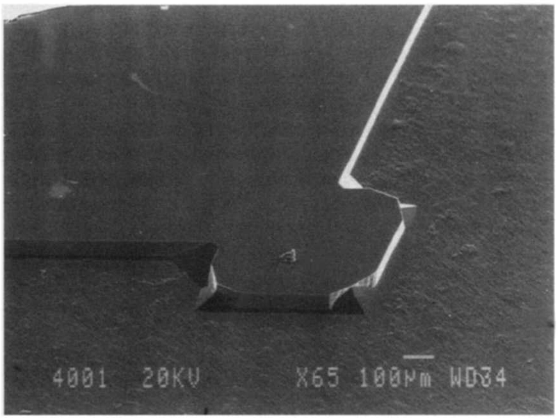

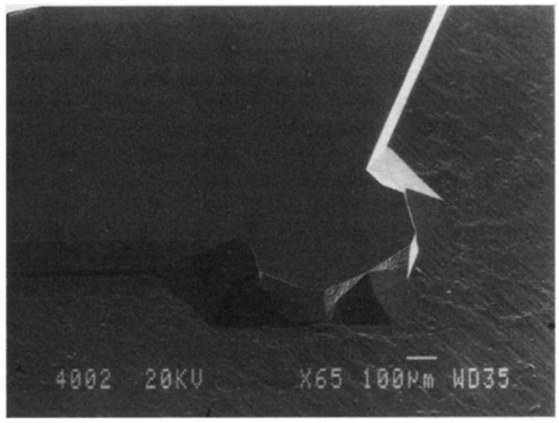

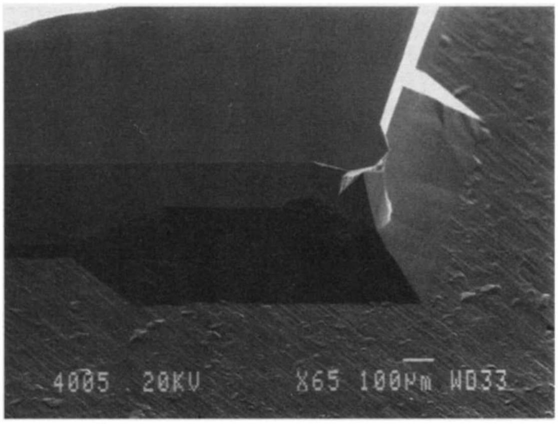

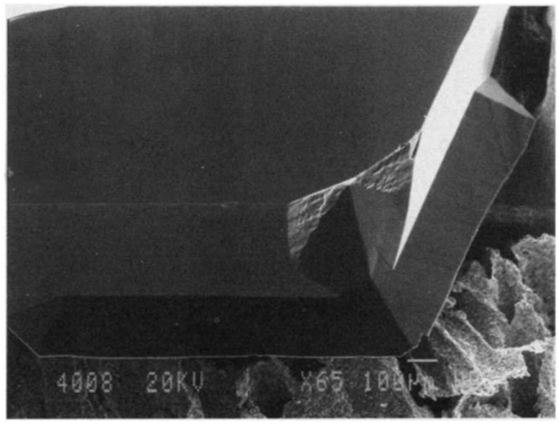

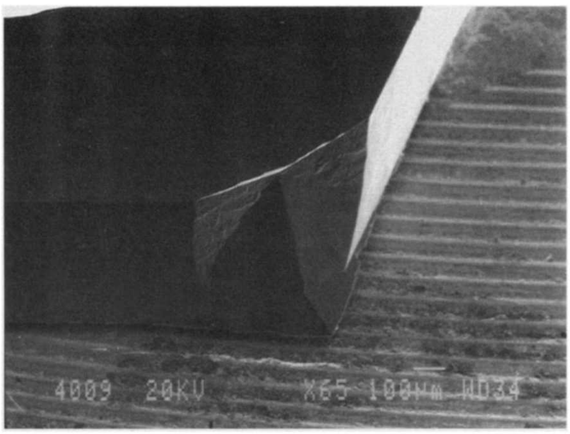

Fig. 14. SEM photographs of obtuse convex corners of parallelogrammic structures compensated with rhombic patterns bounded by four (111) crystal planes in 40% (34 wt %) 70°C KOH after etching for : (a, top left) 1 h, (b, top right) 2 h, (c, middle left) 5 h, (d, above) 8 h, (e, bottom) 9 h.

the (311) and (771) planes. The rhombic corner compensation method resulted in the best results, yielding reasonably well-defined features with small residues on both acute and obtuse corners. On the acute corners, the conventional

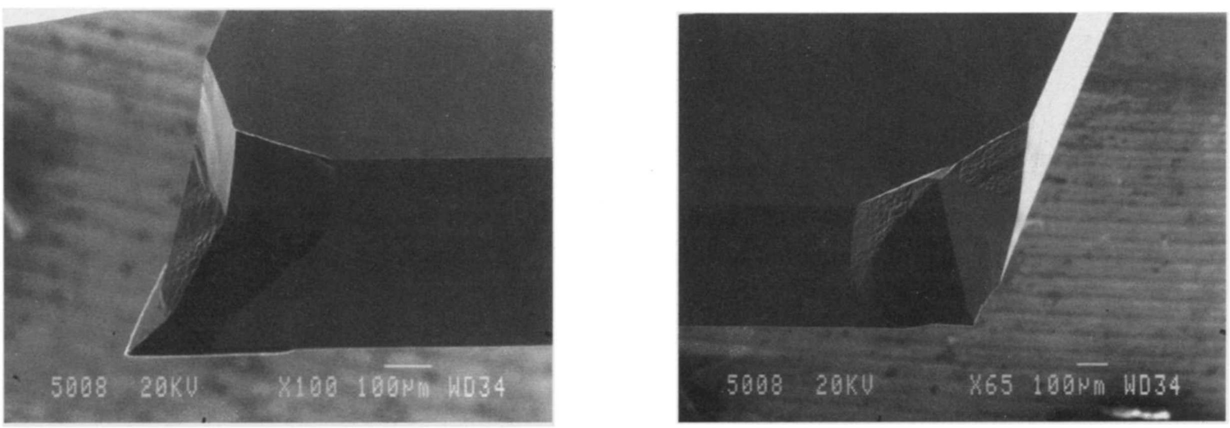

Fig. 15. SEM photographs for rhombic compensation patterns bounded by four (111) crystal planes after 8 h of etching in 50% (42.5 wt %) 80°C KOH. (a, left) Acute convex corner. (b, right) Obtuse convex corner.

<111> corner compensation beams may also be used, but the required corner compensation beam length is longer than the rhombus dimensions.

Manuscript submitted May 27, 1997; revised manuscript received January 26, 1998.

Seoul National University, assisted in meeting the publication costs of this article.

REFERENCES

1. B. Puers and W. Sansen, *Sens. Actuators, A*, **21-23**, 1036 (1990).
2. M. M. Abu-Zeid, *J. Electrochem. Soc.*, **131**, 2138 (1984).
3. H. Sandmaier, H. L. Offereins, K. Kuhl, and W. Lang, in *Technical Digest of Transducers '91*, San Francisco, CA, p. 456, IEEE (1991).
4. M. Bao, C. Burrer, J. Esteve, J. Bausells, and S. Marco, *Sens. Actuators, A*, **37-38**, 727 (1993).
5. G. K. Mayor, H. L. Offereins, H. Sandmaier, and K. Kuhl, *J. Electrochem. Soc.*, **137**, 3947 (1990).
6. H. Seidel, L. Csepregi, A. Heuberger, and H. Baumgartel, *J. Electrochem. Soc.*, **137**, 3612 (1989).
7. D. L. Kendall, *Annu. Rev. Mater. Sci.*, 9, 373 (1979).
8. L. D. Clark, Jr. and D. J. Edell, in *Proceedings of IEEE Micro Robots and Teleoperators Workshop*, Hyannis, MA, Paper 5, IEEE (1987).
9. P. Krause and E. Obermeier, *J. Micromech. Microeng.*, **5**, 112 (1995).
10. Y. Uenishi, M. Tsugai, and M. Mehregany, *J. Micromech. Microeng.*, **5**, 305 (1995).
11. D. R. Ciarlo, *J. Micromech. Microeng.*, **2**, 10 (1992).
12. D. R. Ciarlo, in *Proceedings of the IEEE Micro Robots and Teleoperators Workshop*, Hyannis, MA, Paper 6, IEEE (1987).

Amorphous Hydrogenated Silicon Films for Solar Cell Application Obtained with 55 kHz Plasma Enhanced Chemical Vapor Deposition

B. G. Budaguan,[a] A. A. Sherchenkov,[a] D. A. Stryahilev,[a] A. Y. Sazonov,[a] A. G. Radosel'sky,[a] V. D. Chernomordic,[b] A. A. Popov,[b] and J. W. Metselaar[c]

[a]*Moscow Institute of Electronic Technology, Moscow 103498, Russia*
[b]*Institute of Microelectronics, Russian Academy of Sciences, Yaroslavl' 150007, Russia*
[c]*Faculty of Information Technology and Systems, Delft University of Technology, 2628 CD Delft, The Netherlands*

ABSTRACT

In this work, a-Si:H films with good electronic properties in spite of an inhomogeneous structure were prepared by the 55 kHz plasma enhanced chemical vapor high-rate deposition technique. The structural analysis using infrared spectroscopy and atomic force microscopy has shown that these films possess two dominant types of microstructural inhomogeneities, which differ by size. To analyze the influence of a 55 kHz plasma on the properties of intrinsic a-Si:H film, the density of states in the a-Si:H mobility gap was estimated by modeling of the temperature dependence of the photoconductivity and from electron paramagnetic resonance measurements. Investigated capacitance-voltage characteristics showed that a-Si:H/c-Si heterostructures have low interface density of states and can be considered as an ideal abrupt heterojunction.

Introduction

Amorphous hydrogenated silicon technology is favorable in a wide range of applications. Deposition of a-Si:H films on large areas at relatively high rates and low temperatures is useful for the fabrication of photovoltaic devices. However, from the viewpoint of industrial applications and the production of low cost devices it is essential to increase the a-Si:H deposition rate. The use of 55 kHz plasma enhanced chemical vapor deposition (PECVD) provides a sufficiently increased growth rate of amorphous hydrogenated silicon films compared with that obtained with the commonly used 13.56 MHz PECVD method.[1] However, the possibility of device fabrication using such a-Si:H films has not been studied. On the one hand, it is well known that an increase of the growth rate of a-Si:H films results usually in an increase of structural inhomogeneity and a deterioration of the electronic properties. On the other hand, the increase of ion flux and ion bombardment of the substrate in such a plasma can lead to an increase of the density of states in the growing material and on the a-Si:H/c-Si interface.

In this work, the structural characteristics and electronic properties of undoped a-Si:H films deposited with the 55 kHz PECVD method were investigated in a wide range of technological parameters. To analyze the influence of the 55 kHz plasma on the undoped a-Si:H film the density of states in the mobility gap was estimated by modeling of the temperature dependence of the photoconductivity and from electron paramagnetic resonance (EPR) measurements.

Experimental

Undoped a-Si:H films were deposited in industrial 55 kHz reactor with parallel-plate graphite electrodes. Both electrodes were ungrounded. The source gas was pure SiH_4 (Alphagaz, 99.999%).

The a-Si:H films were deposited on a p-type monocrystalline silicon substrate with a resistivity of 10 Ω cm and on fused silica substrates at low frequency (LF) power of 50 to 400 W (corresponding power density 12.5 to 100 mW/cm^{-2}), gas pressure of 40 to 190 Pa, and growth rate of ~4.2 to 31 Å/s. The substrate temperature was 225°C.

The morphology of the film surface was investigated by atomic force microscopy (AFM) on a P4-SPM-MDT scanning probe microscope. The structure of the film was investigated by AFM and infrared (IR) spectroscopy with the double-beam spectrometer SPECORD M-80. To reveal the presence of microcrystals in deposited a-Si:H films, diffraction analysis with the diffractometer D2 Rigaku Denki was performed.

The density of neutral dangling bonds was measured by electron paramagnetic resonance spectroscopy on samples of 1 μm thickness on quartz substrates.

For dark and photoconductivity measurements, Al coplanar electrodes separated by 0.6 mm were deposited on